IEEE Access
Multidisciplinary | Rapid Review | Open Access Journal

Received September 6, 2019, accepted September 29, 2019, date of publication October 14, 2019, date of current version October 24, 2019.

Digital Object Identifier 10.1109/ACCESS.2019.2946702

Investigation of Ultrasonic Sonotrode Design to Improve the Performance of Ultrasonic Fouling Removal

HABIBA LAIS[1], PREMESH SHEHAN LOWE[2], (Member, IEEE), LUIZ CARLOS WROBEL[1,3], AND TAT-HEAN GAN[4]

[1]Brunel University London, Uxbridge UB8 3PH, U.K.
[2]Nuclear AMRC, Rotherham S60 5WG, U.K.
[3]Pontifical Catholic University of Rio de Janeiro (PUC-Rio), Rio de Janeiro 22451-900, Brazil
[4]TWI Ltd., Cambridge CB21 6AL, U.K.

Corresponding author: Tat-Hean Gan (tat-hean.gan@brunel.ac.uk)

This work was supported by the Engineering and Physical Sciences Research Council under Grant EP/N509097/1.

ABSTRACT Fouling build-up is a well-known industrial problem and its accumulation is dependent on the conditions surrounding the structure. Conventional fouling removal methods are costly and also require an operational halt to carry out the procedure. The use of Ultrasonics has gained popularity in recent years as a non-invasive means of fouling removal but further research and development are required to improve and optimize the technology. Currently in industry, Ultrasonic horns are designed and optimized to generate high amplitude vibrations for various applications including welding, cutting and sonochemistry. Some research has been done to design horns for the generation of cavitation, but none specifically for fouling removal applications. This work investigates the addition of half-wavelength transducer horns of varying shapes (cylindrical, conical, exponential and stepped) to an existing 40 kHz cleaning transducer. Numerical modelling is carried out to optimize the length of the horn before manufacturing final geometries. Experiments were conducted to attach an ultrasonic horn to the transducer and to a carbon steel plate (300 mm $\times$ 300 mm $\times$ 2 mm), and to measure wave propagation across the structure using a PSV-400 3D Laser Scanning Vibrometer. This has shown that the addition of an ultrasonic horn improves the out-of-plane displacement across the structure, which correlates to an improvement in fouling removal for steel tube ultrasonic cleaning.

INDEX TERMS Fouling removal, ultrasonic, finite element analysis, laboratory validation.

I. INTRODUCTION

Fouling build-up is a well-known problem in various industries [1], [2], and its accumulation occurs in different structures such as offshore pipes, ship hulls, floating production platforms. The type of fouling that accumulates is dependent on the environmental conditions surrounding the structure itself.

Conventional fouling removal techniques are costly and time consuming as they require a halt in operations. This has resulted in many attempts to mitigate, monitor and remove this accumulation in a cost-effective manner. As mitigating methods cannot guarantee 100% anti-fouling, removal procedures must be carried out to ensure that the fouled structure does not reach a detrimental state. Current fouling removal methods include chemical, abrasive and hydraulic means, all sharing the common disadvantage of necessitating halting production for the cleaning process to commence.

A non-invasive alternative fouling removal technology which has emerged in recent years is Ultrasound cavitation [3]–[7]. Ultrasonic cleaning is achieved by exciting High Power Ultrasonic Transducers (HPUTs) that generate cavitation bubbles within a surrounding liquid. When the cavitation bubble implodes, the shockwaves produced can dislodge solids attached to a fouled surface. Traditionally, Ultrasound is used in ultrasonic baths to clean a submerged component by the generation and implosion of cavitation bubbles on the fouled surface [8], [9]: this method is particularly used in Reverse Osmosis applications [10], [11]. However, this approach requires the submersion of the fouled structure and

The associate editor coordinating the review of this manuscript and approving it for publication was Yingxiang Liu.

thus may require a halt to production. Large fouled structures such as pipelines cannot be accommodated.

Previous work by the present authors has explored the capability of this technology to remove fouling non-invasively [3]–[7], however further work is needed to enhance the ultrasonic transducers used in this process.

A. APPLICATIONS OF ULTRASONIC SONOTRODES

Currently, industrial transducer-horn attachments are designed to generate high amplitude vibrations for various applications including welding, cutting and sonochemistry.

An in-depth literature review has been carried out in the past to study the various applications of power ultrasound [12] [13]. The industrial uses of power ultrasonics include sterilization of medical equipment, welding of thermoplastics and metals due to *sheer vibration*. The transducers are easily embedded for mass-production automated tools and can be used for composite materials and additive manufacturing. Sonochemistry has benefited from the inclusion of ultrasound for material science, chemistry, biotechnology, cell activation and oxidation. The food industry utilizes ultrasound for the decontamination of water, sterilization, tenderization, freezing, degassing and altering some properties of food.

The development and addition of ultrasonic horns has been used to further the properties of HPUTs to achieve higher amplitude and more precision. This is usually carried out following numerical analysis and theoretical calculation to optimize the design of the horn for its given application. Examples of this include micro-EDM drilling [14], electro-discharge machining [15], flange making [16], grinding [17], plastic welding [18], ultrasonic machining [19].

Aside from these applications, other purposes of the transducer enhancement include achieving multi-frequency transduction [20] and improvement of velocity amplification [18], [21]. Another enhancement is the addition of diagonal slits on horns to promote longitudinal-torsional wave modes [22].

Ultrasonic horns are typically designed to a *geometrical iteration* of half a wavelength in length to achieve maximum amplitude at the contact surface of the horn tip [23]. Horns can be found of simple shapes such as cylindrical, conical, stepped or exponential diameter variation [18], [21], or as a combination of these different shapes [14].

The magnitude of amplification is increased in line with the ratio of the horn diameter to its tip diameter. Each shape contributes different amplitude characteristics, such as the filtering of noise, increased amplitude and achieved non-contact performance. Combinations of these shapes have been investigated to further improve the performance for given applications.

Literature shows many attempts to improve amplification through the use of Ultrasonic horns, but there is no previous work related to the improvement of fouling removal applications. Research that is most similar to improving fouling removal properties has been into ultrasonic horns that can generate and enhance cavitation intensity. Cavitation activity from ultrasonic horns has been investigated using COMSOL [24]–[26]. For example, sonochemistry enhancement by the generation of cavitaton for oxidation [27]. As Ultrasonic horns have the potential to generate cavitation for sonochemical applications, this suggests the prospect for improving the non-invasive ultrasonic cleaning technique by increasing its cleaning distance.

This present work investigates the development of different Ultrasonic horn geometries and studies improvements in the wave propagation across a plate structure. This is carried out by designing a half-wavelength ultrasonic horn within COMSOL (with cylindrical, conical, exponential and stepped shapes). The ultrasonic horns are designed with a threaded piece for attachment onto an existing 40 kHz HPUT. The transducer is attached at the center of a carbon steel plate (300 mm × 300 mm × 2 mm), and is excited using a discrete pulse. A PSV-400 3D Laser Scanning Vibrometer is used to measure the displacement across the plate structure over time. The ultrasonic sonotrode with highest improvement of wave propagation is used to carry out an FEA analysis to predict improved cleaning capabilities compared to a single transducer. A cleaning trial is carried out on an 85 mm length, 50.08 mm outer diameter and 1.5 mm wall thickness, stainless steel pipe which is filled with water. The cleaning achieved for the selected sonotrode is compared with the results for a single transducer.

II. HIGH POWER ULTRASONIC TRANSDUCERS

The most common type of piezoelectric transducer is known as the *Langevin transducer*. This HPUT consists of piezoelectric ceramic ring elements that are stacked and sandwiched between electrodes and are pre-stressed using a front and back mass (Figure 1). HPUTs are fabricated by bolting the front and back masses, and by placing stacked piezoelectric ceramic rings (1/8th wavelength each) between both masses before bolting. The material used for these components varies depending on the desired mechanical and chemical properties of the transducer, and are listed below:

- Two piezoelectric ceramic rings (compressional) – 1/8 wavelength length
- Two contact plates
- Front mass – 1/2 wavelength length

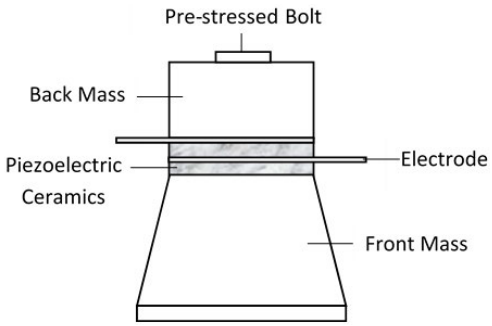

FIGURE 1. Diagram of HPUT components.

- Back mass – 1/4 wavelength
- Bias bolt with nut – 1/4 wavelength length
- Insulating tubing for bolt
- Epoxy resin - as adhesive and acoustic couplant between each component

The purpose of the back mass is to boost the vibration of the transducer towards the front mass. A common method to achieve this is to select an appropriate backing mass geometry and a material that has a higher acoustic impedance.

A. LONGITUDINAL VIBRATIONS

To understand the vibration behavior of a designed mechanical horn, vibration in bars of circular cross-section must first be understood [28]. To calculate the longitudinal vibration in bars, the stress-strain formula can be used, where strain is given by:

$$\epsilon = \frac{\partial \omega}{\partial x} \tag{1}$$

The stress is given by

$$\frac{F}{S} = -E \cdot \epsilon, \tag{2}$$

where ω is the displacement along the bar, x is the distance, S is the cross-section of the bar, F is the force and E is the Young's modulus.

Using the stress and strain equations, the longitudinal wave equation is as follows:

$$\frac{\partial^2 \omega}{\partial x^2} = \frac{1}{c_L^2} \frac{\partial^2 \omega}{\partial t^2}, \tag{3}$$

where c_L is the velocity of the longitudinal vibration, calculated using the following equation:

$$c_L = \sqrt{\frac{E}{\rho}}, \tag{4}$$

where ρ is the density of the material.

Assuming the cylindrical bar is free at both ends, its mode shape can be calculated using the equation:

$$\omega(x, t) = 2We^{j\omega_n t} \cos(k_n x), \tag{5}$$

where W is the amplitude of the vibration , k_n is the wave number and ω_n is the angular frequency of the n^{th} resonance.

The n^{th} resonant frequency can be calculated using the equation [29]:

$$f_n = \frac{nc_L}{2L}, \tag{6}$$

where L is the length of the bar.

The first resonance is also known as the half-wavelength resonance and is typically the length used to design the front mass of HPUTs.

III. NUMERICAL INVESTIGATION

The HPUT model was implemented in COMSOL 5.4 and neglects the contact plates and epoxy resin within the transducer. Instead, the voltage is applied directly to the faces of the piezoelectric ceramic rings. The model uses the HPUT dimensions in Figure 2 and the material properties in Table 1. The piezoelectric ceramic rings are made of PZT-4 and their material properties are selected from the built-in database in COMSOL [30].

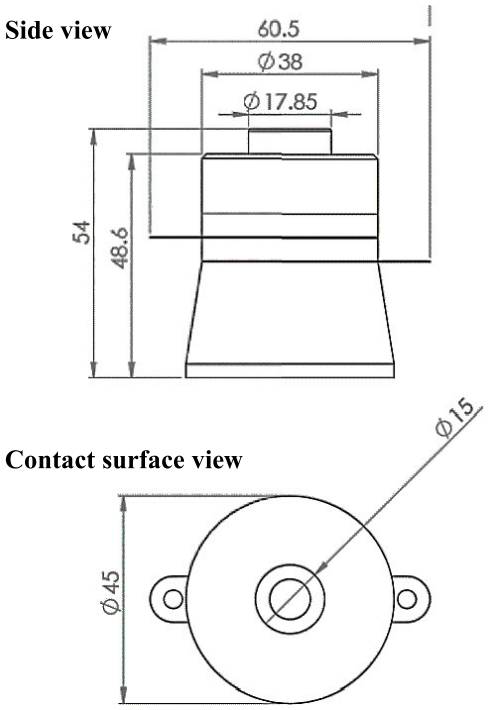

FIGURE 2. Dimensions of Selected 40 kHz HPUT.

TABLE 1. Metallic component material properties.

Material Property	Aluminum	Stainless Steel
Density	2700 kg/m^3	7830 kg/m^3
Young's Modulus	70 x 10^9 Pa	207 GPa
Poisson's Ratio	0.35	0.3

A. PHYSICS

Linear elastic behavior is assumed for all solid parts of the model, excluding the piezoelectric ceramic rings. The application of Newton's law yields the following equation:

$$\rho_S \frac{\partial^2 \boldsymbol{u}}{\partial t^2} = \boldsymbol{\nabla} \cdot \overline{\overline{\mathbf{T}}} \tag{7}$$

where, $\boldsymbol{u}$ is the solid displacement field, $\overline{\overline{T}}$ is the stress tensor, and ρ_S is the density of the solid.

A piezoelectric material is assigned to the piezoelectric ceramic rings which obey the solid mechanics governing equations and, additionally, the PZT- linearized constitutive

equations in stress-charge form:

$$\overline{\overline{\mathbf{T}}} = c_E \cdot \overline{\overline{S}} - e^t \cdot \boldsymbol{E} \tag{8}$$

$$\mathbf{D} = e \cdot \overline{\overline{S}} + \varepsilon_S \cdot \boldsymbol{E} \tag{9}$$

where, $\overline{\overline{T}}$ is the stress tensor, $\overline{\overline{S}}$ is the strain tensor, $\boldsymbol{E}$ is the electric field, $\boldsymbol{D}$ is the electric displacement field, c_E is the elasticity matrix, e is the piezoelectric coupling coefficient for the stress-charge form and ε_S is the permittivity matrix.

Electrostatic behaviors are assigned to the piezoelectric ceramic rings with the signal applied using the formulae:

$$\nabla \cdot \mathbf{D} = 0 \tag{10}$$

$$\mathbf{E} = -\nabla V \tag{11}$$

where$V$ is the electric potential corresponding to the electric field $\boldsymbol{E}$.

The terminal and ground equipotentials are applied to the boundaries explicitly as in previous work [4]. The ground boundary is set to 0 V and the terminal boundary is set to:

$$V = V_0 \tag{12}$$

where *Vo* is the modulated input signal. The correct polarization is achieved by assigning a rotated global co-ordinate system to one of the two piezoelectric ceramic rings and rotating its polarization towards the second piezoelectric ceramic ring.

B. MESH

A dynamic transient simulation to map out the wave propagation requires the calculated mesh to be optimal. The wave equation requires the time stepping within the solver to complement the meshing itself to yield an accurate solution. The meshing size uses ten 2nd-order elements per wavelength. The equation used to calculate the maximum allowed mesh element size (*ho*) is given by [31]:

$$h_o = \frac{c}{Nf_o}$$

$$h_o = \frac{2700}{10 \times 40000} = 0.00675m \tag{13}$$

where c is the group velocity, N is number of elements per wavelength and f_0 is the centre frequency.

The 40 kHz HPUT undergoes analysis using the Agilent 4294A Precision Impedance Analyzer [32]. Figure 3 shows an experimental impedance of 18.51 Ω at 39.98 kHz and a numerical impedance of 9.72 Ω at 39.60 kHz. The HPUTs were purchased from Beijing Ultrasonics [33] which states the impedance of the HPUT to be 40 kHz ± 1kHz, which means that the numerical model is in good agreement to the resonating frequency. The variation in impedance is due to neglecting the electrode contact plates within the numerical methodology.

C. EIGENFREQUENCY ANALYSIS

The HPUT model is simulated as 2D axisymmetric and undergoes eigenfrequency analysis as shown in Figure 4.

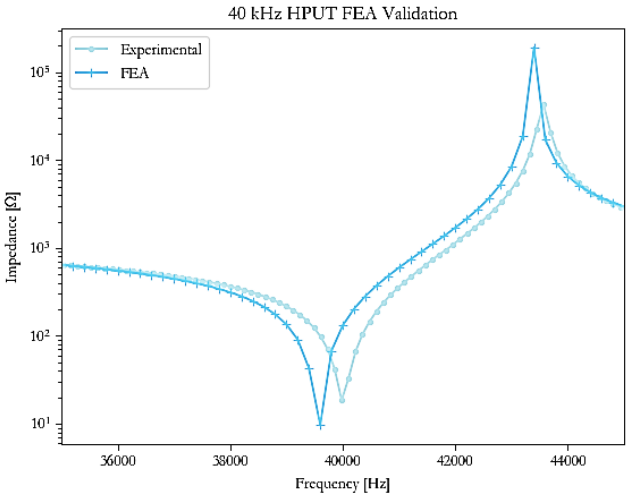

FIGURE 3. HPUT impedance comparison of experimental and numerical results.

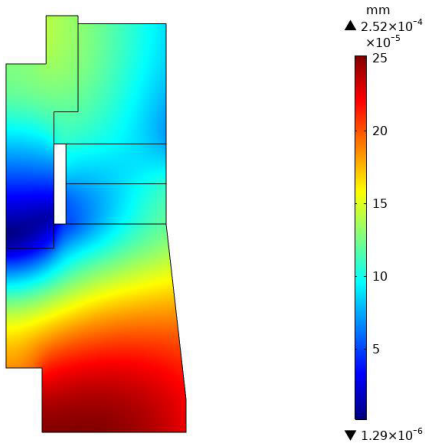

FIGURE 4. Displacement distribution at resonant frequency (40 kHz).

The maximum displacement achieved across the HPUT is localized at the transducer contact surface.

IV. TRANSDUCER SONOTRODE DESIGN

The transducer horns are designed to have a total length equivalent to half a wavelength, calculated by using the fundamental equations below and the material properties of the desired ultrasonic horn. Ultrasonic horns are designed in aluminum to match the material of the front mass of the HPUT. Using the equations below, the length of the ultrasonic horn is calculated as 0.0636 m as follows:

$$L_{Horn} = \frac{\lambda}{2} \tag{14}$$

$$\lambda = \frac{c_L}{f}$$

$$L_{Horn} = \frac{\lambda}{2} = \frac{c_L}{2f} = \frac{\sqrt{\frac{E}{\rho}}}{2f} = \frac{\sqrt{\frac{70\times10^9}{2700}}}{2 \times 40000} = 0.0636m \tag{15}$$

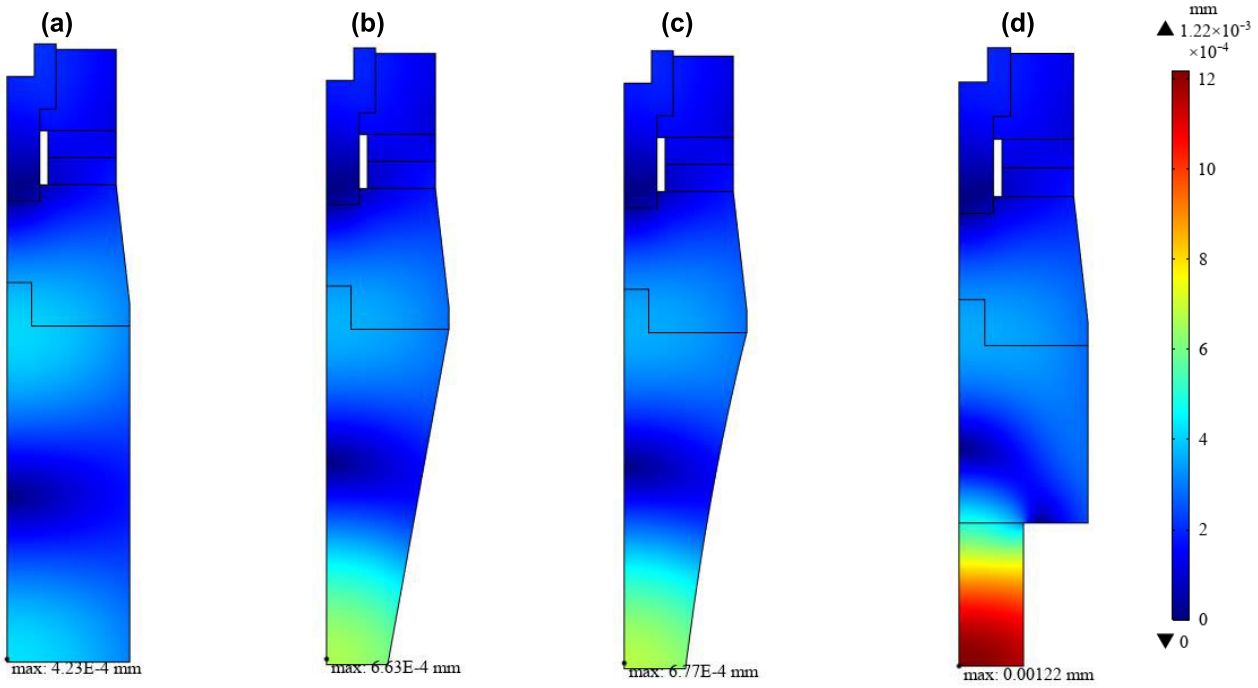

FIGURE 5. Displacement distribution across 40 kHz HPUT with (a) cylindrical, (b) conical, (c) exponential and (d) stepped ultrasonic horns attached.

where L_{Horn} is the length of the ultrasonic horn and λ is the wavelength.

Excluding the cylindrical horn, which has a constant diameter throughout its length, the ultrasonic horns are designed to have a *magnification factor* of 2 at the horn tip. This means that the diameter at the tip of the horn is half the diameter in contact with the HPUT surface. The conical horn has a linearly varying diameter along its length. The stepped horn comprises two quarter-wavelength cylinders, the first quarter matching the diameter of the HPUT contact surface and the second part is half the diameter of the HPUT contact surface, resulting in a *magnitude* of 2. The diameter of the exponential horn varies along its length according to the equation:

$$S(x) = S_1 e^{-kx} \tag{16}$$

$$k = \frac{-ln\left(\frac{D_2}{D_1}\right)}{L}$$

$$k = \frac{-ln\left(\frac{1}{2}\right)}{0.0636} = 10.89 \tag{17}$$

where S is the surface area, k is the taper factor, D is the diameter, L is the length. Subscript 1 refers to the input/wider part of the ultrasonic horn and subscript 2 refers to output/narrower part of the ultrasonic horn

A. NUMERICAL INVESTIGATION

Each horn is designed in COMSOL using the equations appropriate to each ultrasonic horn geometry. A parametric study was conducted on the length of the ultrasonic horn to adjust the geometry to achieve an eigenfrequency close to 40 kHz. The numerical analysis of each ultrasonic horn is shown in Figure 5. The cylindrical horn shows high displacement at the original HPUT contact surface and at the tip of the ultrasonic horn, confirming that the addition of the half-wavelength horn achieves double the displacement of the HPUT in Figure 4.

The conical horn shows much higher displacement at the horn tip compared to the original contact surface, and is higher than for the cylindrical horn, showing that the *magnitude* at the horn tip improves the amplitude. The exponential horn gives a similar result to the cylindrical horn but shows minor increases in the displacement. This can be due to having a similar diameter variation along the length of the horn as a result of the selection of horn magnitude. The stepped horn shows the largest increase in displacement at the horn tip, possibly due to the geometry achieving optimal filtering and focusing of the HPUT vibration.

V. EXPERIMENTAL INVESTIGATION

The final ultrasonic horn geometries are shown in Figure 6 and were manufactured with a threaded component for interchangeability (Figure 7). Each ultrasonic horn is attached to the 40 kHz HPUT and undergoes analysis using the Agilent 4294A Precision Impedance Analyzer [32], with the results shown in Figure 8. The 40 kHz HPUT (flat) achieves the lowest impedance at its resonant frequency. With the addition of an ultrasonic horn, the added mass results in an increase in impedance as well as additional resonant and anti-resonant

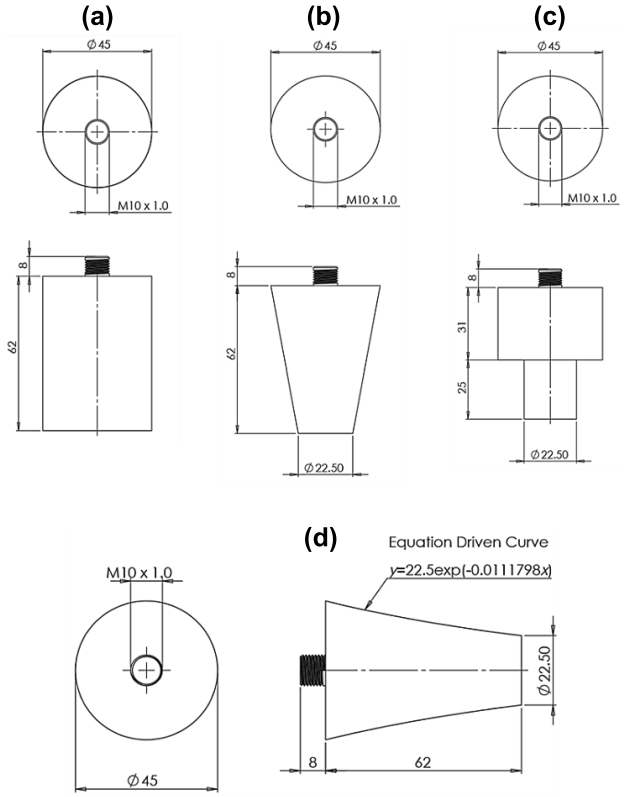

FIGURE 6. Geometry of (a) cylindrical, (b) conical, (c) stepped and (d) exponential shaped ultrasonic horns.

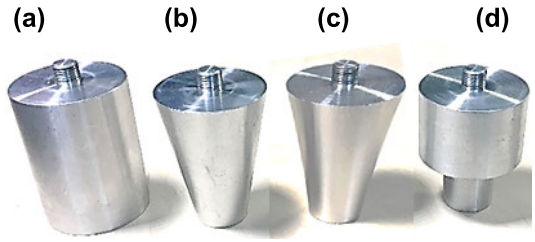

FIGURE 7. Manufactured (a) cylindrical, (b) conical, (c) exponential and (d) stepped ultrasonic horn.

responses for the stepped horn. The horns also shift the natural frequency, thus numerical analysis and parametric optimization were used to maintain a resonant frequency close to 40 kHz. When comparing the impedance achieved from the manufactured sonotrodes to the numerical impedance calculated in Figure 9, good agreement is obtained for each of the sonotrodes excluding the stepped horn, which has the highest impedance at resonance. This is due to the change in diameter of the horn at the stepped section and also due to this horn being shorter than the other three sonotrodes under investigation, which produce an additional resonant and anti-resonant response.

A. WAVE PROPAGATION INVESTIGATION

A 300 mm × 300 mm × 2 mm carbon steel plate is placed within an upright frame as shown in Figure 10. The frame

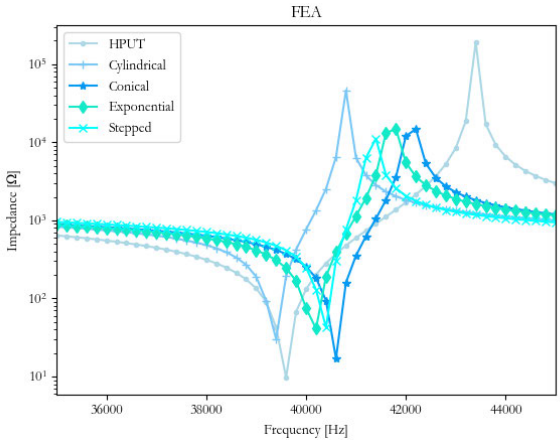

FIGURE 8. Comparison of numerical impedance for final ultrasonic horn designs.

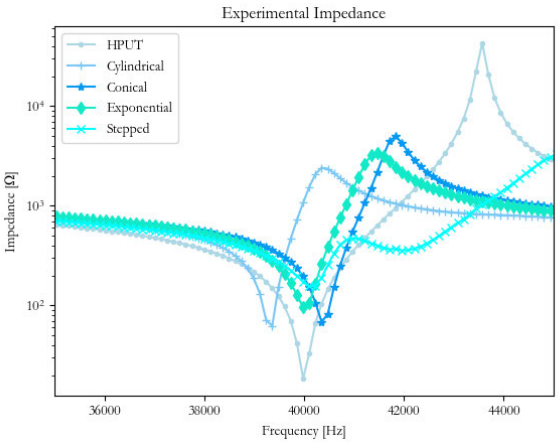

FIGURE 9. Comparison of experimental impedance for final manufactured ultrasonic horn designs.

holds the 40 kHz HPUT and pressurizes the transducer against the centre of the plate. A Polytec PSV-400 3D Laser Scanning Vibrometer [34] is used to scan the outer surface of the plate structure. For this to be achieved, the plate is placed at an optimal distance using the equation:

$$Distance = 0.099 + (n_x \times 0.204) \tag{18}$$

where n_x is the iteration of the optimal distance between the PSV-400 and the test specimen.

The PSV-400 was calibrated to scan the plate where surface preparation is applied. The HPUT is excited using a discrete pulse, which is a 5-cycle sinusoidal wave modulated using the Hann window function as follows:

$$U(t) = \frac{1}{2}\sin(2\pi ft)\left[1 - \cos\left(\frac{2\pi ft}{N}\right)\right] \tag{19}$$

where t is time, f is the central frequency and N is the number of cycles.

Figure 11 shows a high amplitude displacement propagating from the transducer location. For comparison between the horns, the maximum value at the transducer location

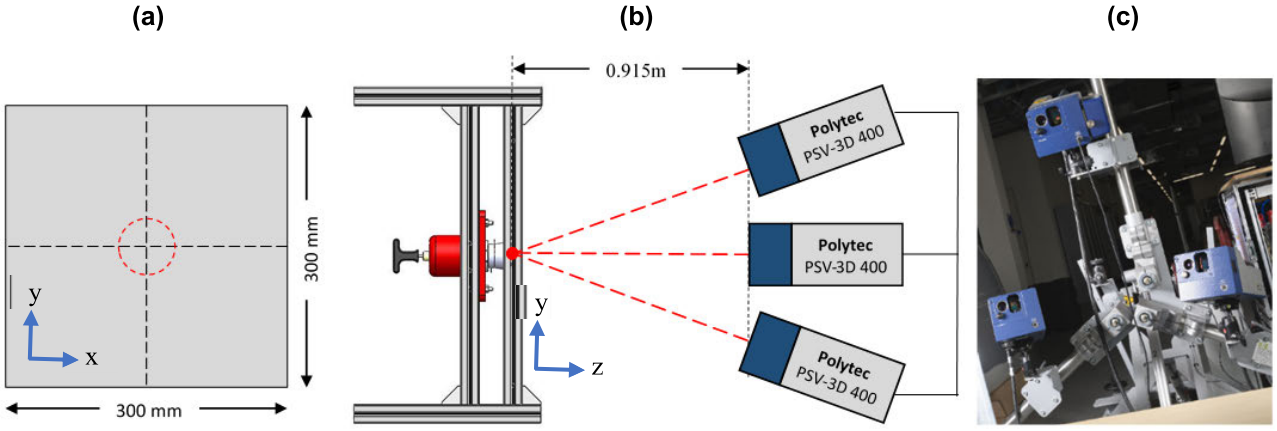

FIGURE 10. (a) Dimensions of 2 mm thick carbon steel plate and location of transducer attachment, (b) experimental set-up for vibrometry analysis and (c) Polytec PSV-400 3D Laser Scanning Vibrometer.

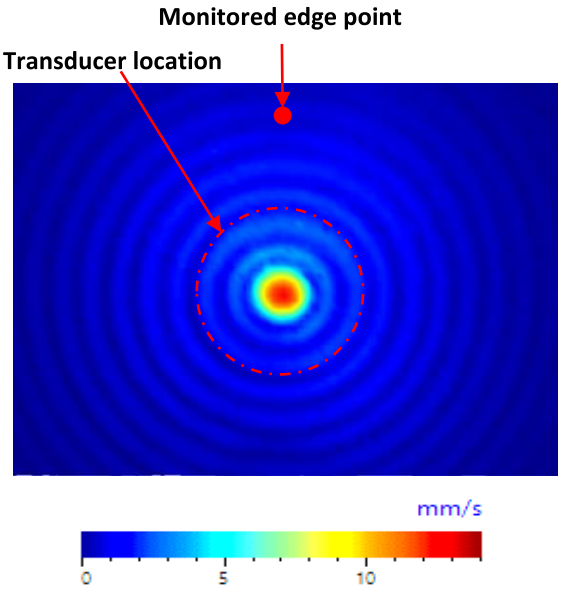

FIGURE 11. HPUT with conical ultrasonic horn attached to center of plate undergoing data collection using 3D Laser Scanning Vibrometer, displaying high amplitude at transducer location.

as annotated in Figure 11 is used. To compare the wave propagation across the plate, the edge point is taken as the maximum value from the furthest ripple from the transducer pulse. At each of these points, the x (displacement along the height of the plate), y (displacement along the width of the plate) and z (out-of-plane displacement, perpendicular to the plate) components are monitored. The component axis is annotated in Figure 10.

When exciting the HPUT, a compressional vibration is generated across the piezoelectric ceramic rings, resulting in vibration perpendicular to the HPUT front mass. The discrete pulse generates vibration in both directions from the piezoelectric ceramic rings, as shown in Figure 12. The vibration will follow a path of propagation in the form of a wave packet. Wave packet 1 describes the first pulse to be received at the

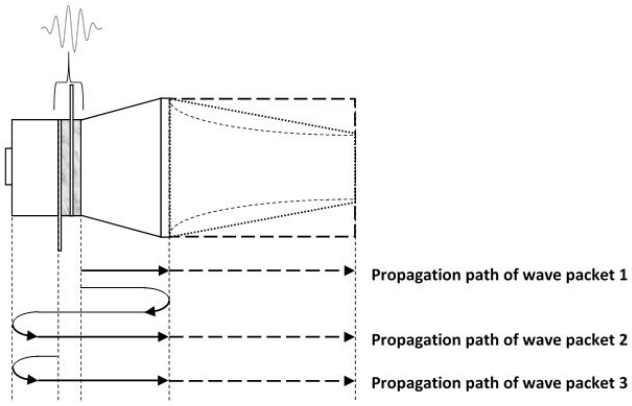

FIGURE 12. Diagram of HPUT propagation paths when excited by a discrete pulse.

HPUT contact surface. Depending on the efficiency of the transducer, some double reflection from the HPUT contact surface and back mass will occur and result in a second wave packet 2, returning to the HPUT, where it is expected to have reduced amplitude compared to wave packet 1. Wave packet 3 is the backward propagating vibration from the initial pulse, reflected at the back mass, and resulting in some reduced signal on arrival at the HPUT contact surface. Further wave packets are produced as a result of multiple signal reflections across the transducer, with reduced amplitude after each reflection. Each wave packet can be identified by the delay of the signal.

1) HPUT

At the transducer location, Figure 13 shows a high out-of-plane (z direction) velocity. The annotated section A relates to wave packet 1 as described in Figure 12. Section B shows a combination of two reflections overlapping, related to wave packets 2 and 3. Over time, the discrete pulse is reflected from the plate edge and is annotated in Figure 13. The x and y components of the signal follow a similar amplitude pattern and result from a compressional excitation of the plate structure.

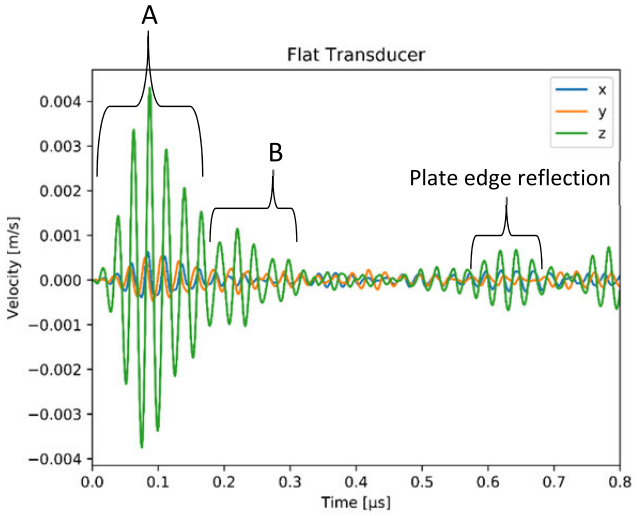

FIGURE 13. Velocity at transducer location for HPUT without ultrasonic horn.

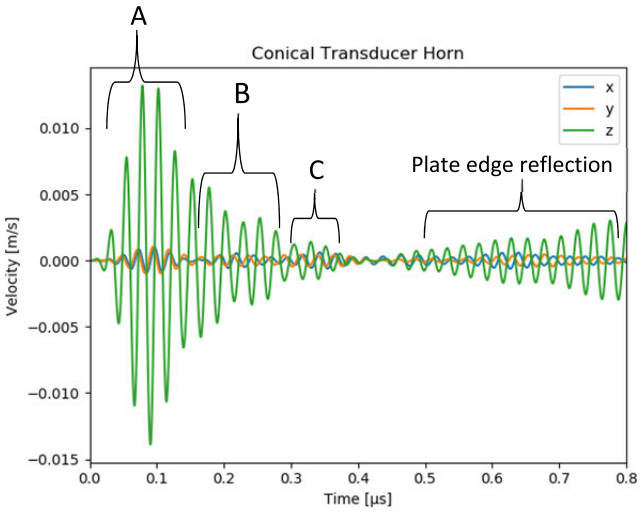

FIGURE 15. Velocity at transducer location for HPUT with conical ultrasonic horn.

2) CYLINDRICAL

The cylindrical horn (shown in Figure 14) achieves 30% higher amplitude in the z-direction at section B compared to the HPUT. Although the transducer is excited using a discrete pulse, the signal is oscillating through the structure due to multiple structure reflections and the lack of filtering of the signal due to the horn geometry. Wave packet 1 (section A) is overlapped by section B, which is a combination of multiple reflections including wave packets 2 and 3. The remainder of the signal (for example section C) shows a reduction in oscillation as the discrete pulse propagates away from its source. This configuration improves the amplitude of the HPUT only due to the addition of wave packets at section B.

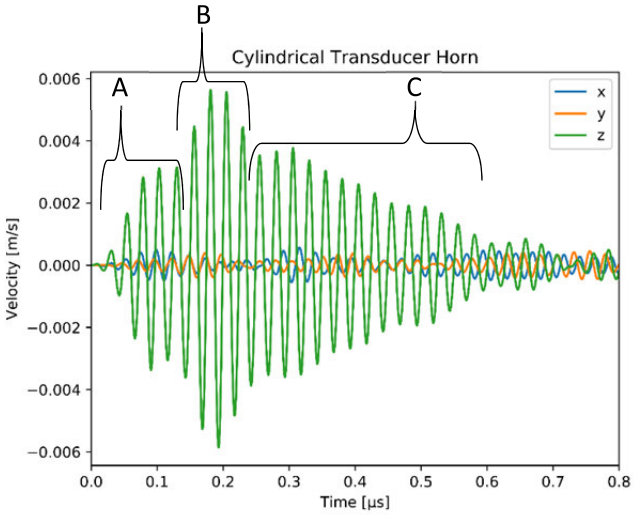

FIGURE 14. Velocity at transducer location for HPUT with cylindrical ultrasonic horn.

3) CONICAL

Figure 15 shows an increase in amplitude (three times the HPUT) of wave packet 1 (section A), which means that the geometry has improved the initial wave packet pulses. Section B is again a combination of wave packets 2 and 3. Section C is a result of an additional reflection generated by the horn geometry. The plate edge reflection can be seen in the figure; however, this is oscillating which may be due to the increased amplitude and additional wave packet reflections.

4) EXPONENTIAL

The amplitude of wave packet 1 shown in Figure 16, section A is increased by 50% compared to the HPUT. However, this is not as high as achieved using the conical horn. Again in the figure, section B is a combination of wave packets 2 and 3. Section C is a result of reflections from the addition of the exponential horn which oscillates for a longer period of time compared to the conical horn. There is very little reflection from the plate edge, possibly due to the lower amplitude achieved using this horn shape.

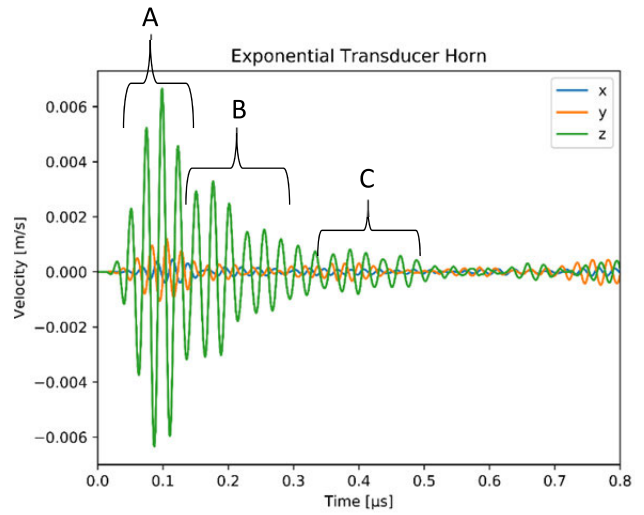

FIGURE 16. Velocity at transducer location for HPUT with exponential ultrasonic horn.

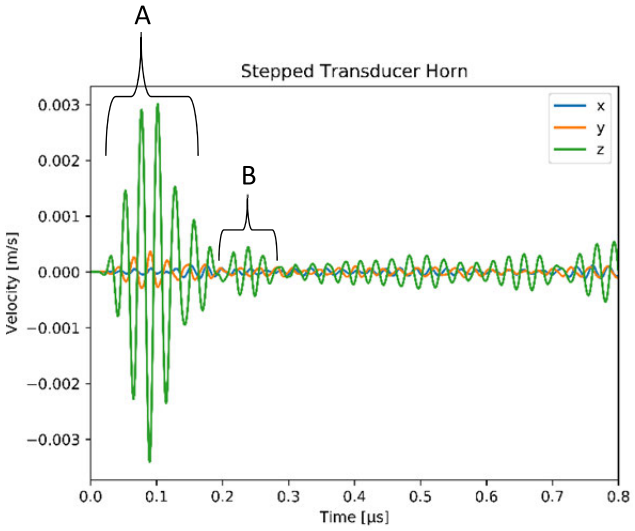

FIGURE 17. Velocity at transducer location for HPUT with stepped ultrasonic horn.

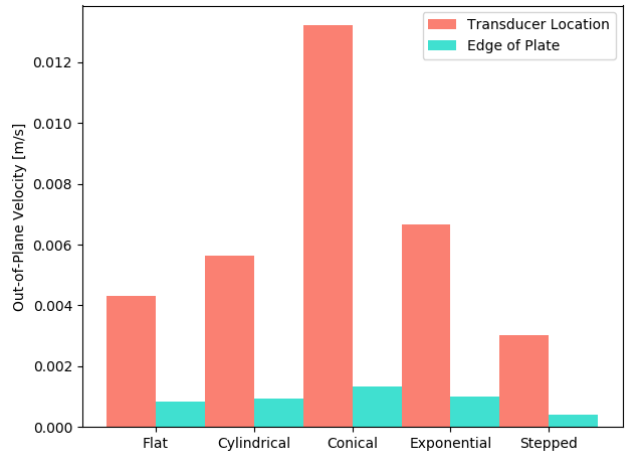

FIGURE 18. Comparison of maximum out-of-plane velocity for each ultrasonic horn.

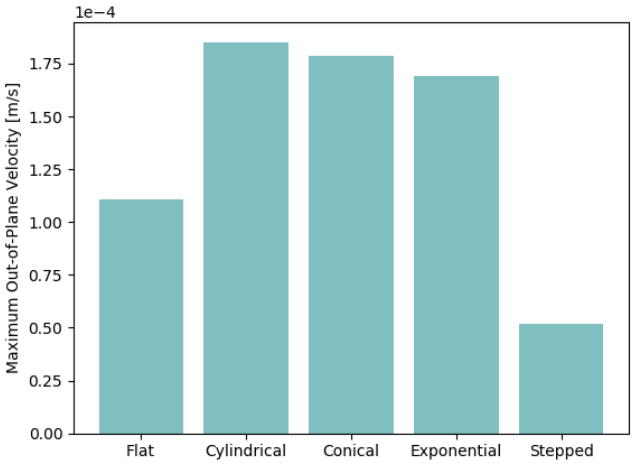

FIGURE 19. Comparison of FFT of ultrasonic horns.

Exponential horns were designed for improved amplitude of the longitudinal mode whilst filtering other components of the signal. As they are typically not designed to be attached

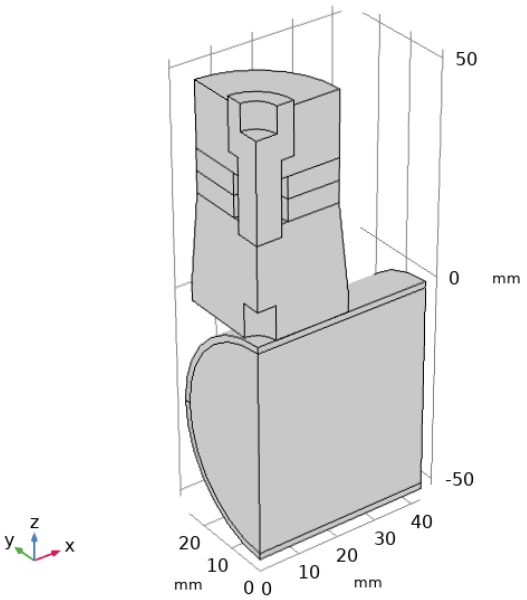

FIGURE 20. Geometry of FEA model for single HPUT, displaying cut planes at lines of symmetry for computational efficiency.

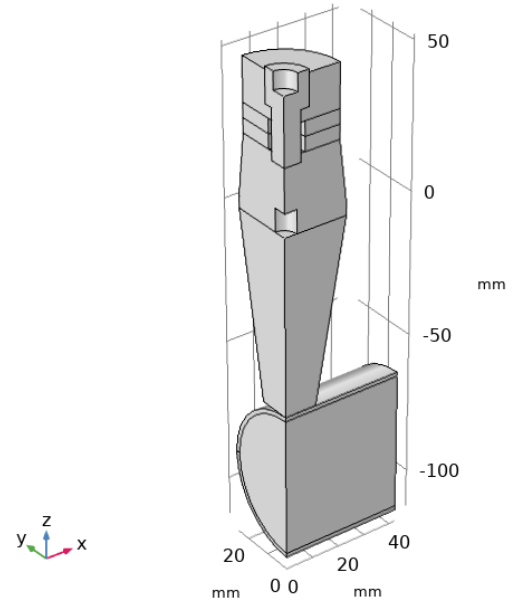

FIGURE 21. Geometry of FEA model for conical sonotrode attached to a single HPUT, displaying cut planes at lines of symmetry for computational efficiency.

onto a plate structure, the reduction in the x and y components of the vibration and the addition of the plate has resulted in attenuation of the signal across the plate.

5) STEPPED

The stepped horn shows a 30% reduction in the velocity (Figure 17) but an improvement of the signal delivery as wave packet 1 (section A) and wave packet 2 (section B) are now separated. The removal of wave packet 3 is due to the geometry of the horn which filters reflected signals. Separation of these signals is beneficial for some applications. However, for ultrasonic cleaning, the HPUT would be

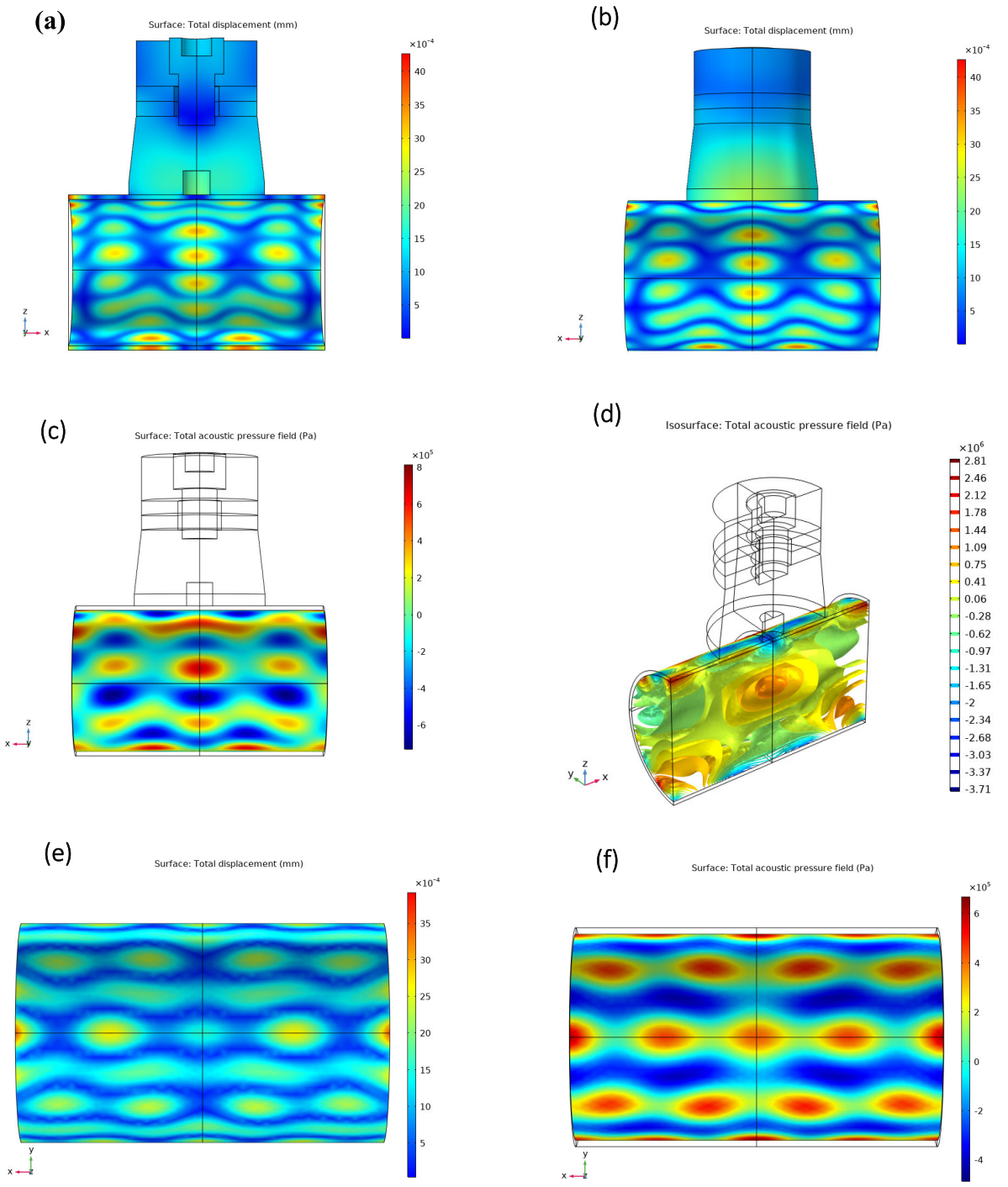

FIGURE 22. FEA results of HPUT on pipe specimen for fouling removal displaying (a) solid displacement on inner pipe wall, (a) solid displacement on outer pipe wall, (c) total acoustic pressure of fluid at inner pipe wall, (d) cross-sectional isosurface view of total acoustic pressure at center of fluid, (e) total displacement of outer pipe wall furthest from HPUT attachment location and (f) total acoustic pressure of fluid at the inner pipe wall furthest from HPUT attachment location.

driven at a continuous sinusoidal waveform so they will not be separable.

The numerical results show the stepped horn should achieve the highest displacement but this was not experimentally achieved in the laboratory investigation. This may be due to the attachment of the plate which attenuated the delivery of the signal and also dampened the vibration of the ultrasonic horn.

6) COMPARISON OF ULTRASONIC HORNS

The conical horn achieved the highest increase in amplitude at the transducer location (Figure 18), and the cylindrical

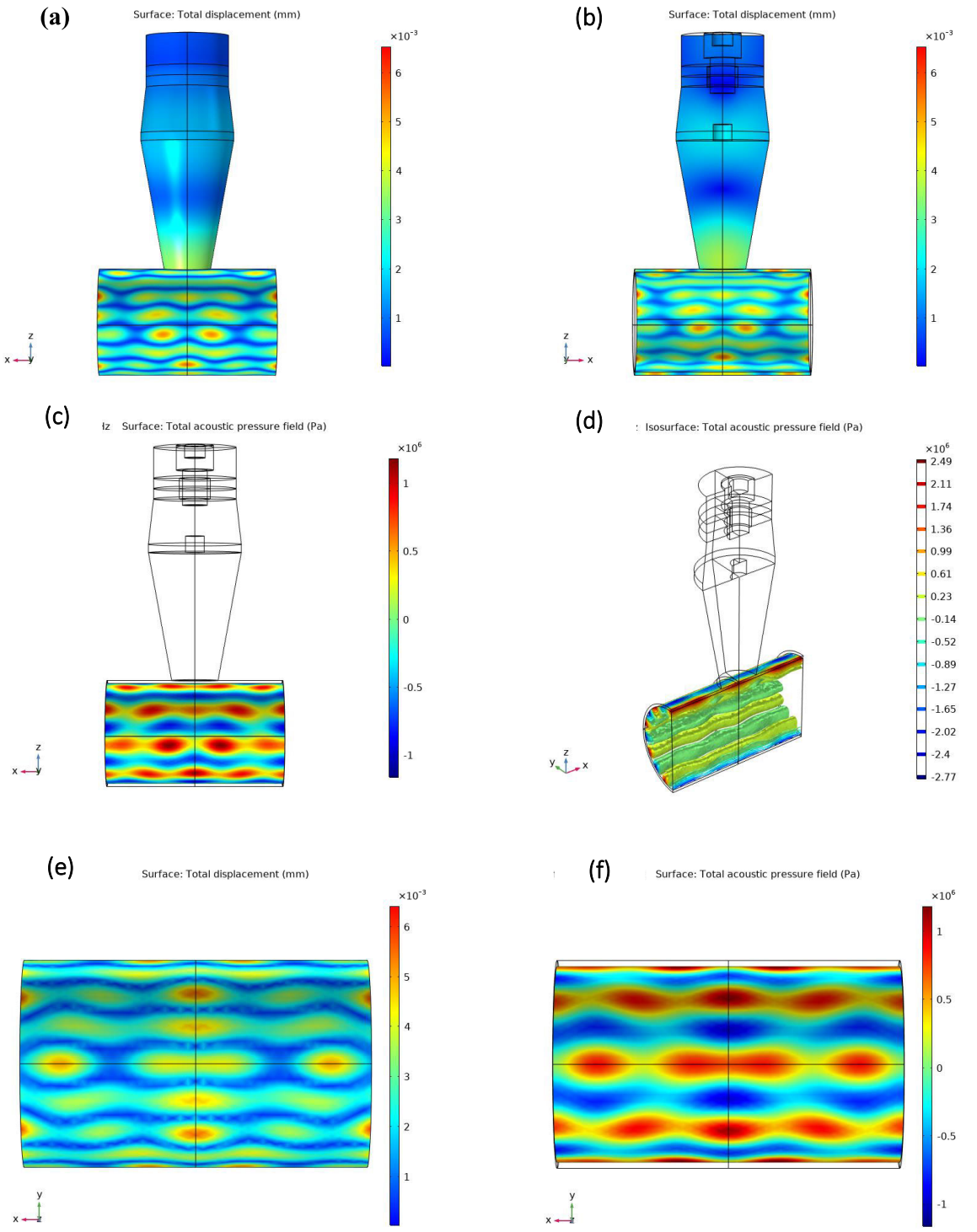

FIGURE 23. FEA results of conical sonotrode on pipe specimen for fouling removal displaying (a) solid displacement on inner pipe wall, (a) solid displacement on outer pipe wall, (c) total acoustic pressure of fluid at inner pipe wall, (d) cross-sectional isosurface view of total acoustic pressure at center of fluid, (e) total displacement of outer pipe wall furthest from conical sonotrode attachment location and (f) total acoustic pressure of fluid at the inner pipe wall furthest from conical sonotrode attachment location.

and exponential horns improved the performance compared to the HPUT. The stepped horn showed a reduction of 30% compared to the HPUT. The velocity achieved at the edge monitored point (refer to Figure 11) follows a similar trend of improvements and reductions.

Another factor that can improve or reduce the amplitude across the plate is the x and y components generated from the horn. As the HPUT has a conical shape, *x* and *y* vibrations are generated across the plate, whereas the filtering of the signal with the exponential and stepped horns minimizes the *x* and *y*

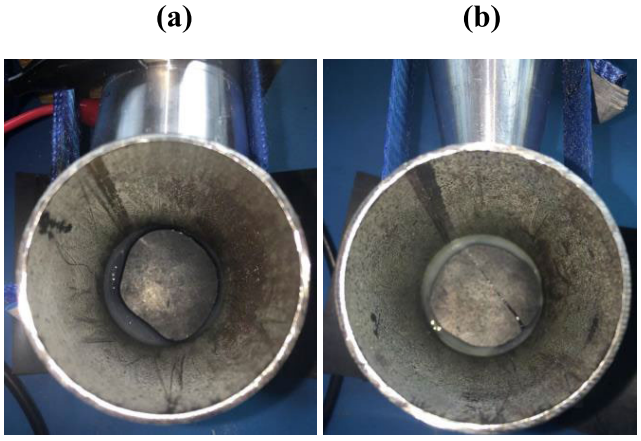

FIGURE 24. Images before cleaning of pipe specimen with (a) 40 kHz HPUT attached and (b) conical sonotrode attached.

components and reduces their propagation once the horns are attached onto the plate.

The data at the transducer location is converted to an FFT (Figure 19) showing highest amplitudes for the cylindrical horn. This is a result of the multiple reflections produced by this horn attachment. The stepped horn has achieved the lowest amplitude, this is due to the filtering of the signal shown in Figure 17.

VI. APPLICATION OF SELECTED SONOTRODE FOR FOULING REMOVAL

From comparing each of the sonotrode designs, the cylindrical sonotrode has shown the highest potential to achieve cleaning improvements due to the increase in displacement across the carbon steel plate structure.

A. NUMERICAL METHODOLOGY

The HPUT and conical sonotrode are modelled in 3D using the validated FEA model as previously discussed in this work.

Each transducer is attached to the center of an 85 mm length, 50.08 mm outer diameter and 1.5 mm wall thickness, stainless steel pipe which is filled with water. Symmetry is used to compute 4 of the model as shown in Figure 20 and Figure 21.

In addition to the solid mechanics, electrostatics and piezoelectric effects are used to define the physics of the model. Pressure acoustics is applied to the fluid domain and acoustic-structure interaction is applied to the inner wall of the pipe in contact to the fluid domain. Integration is applied at the contact surface of the HPUT to couple it to the pipe structure. The results are computed in the frequency domain.

B. NUMERICAL RESULTS

Figure 22 shows the HPUT achieves the minimum pressure required for generating cavitation within a fluid for a 40 kHz HPUT. The displacement displayed shows the potential cleaning patterns achieved from a cycle of cleaning. The HPUT delivers high pressure into the liquid as shown from the isosurface plot, displaying high pressure at the center of the fluid.

Figure 23 shows the conical sonotrode achieving high pressure within the fluid compared to the HPUT. The pressure in the fluid is shown to be distributed against the inner wall of the pipe. This shows the potential focusing of cavitation generation regions.

C. EXPERIMENTAL VALIDATION

To further improve the ultrasonic cleaning technique, the potential of the conical sonotrode for ultrasonic cleaning improvements is demonstrated in this section. A feasibility trial is carried out on an 85 mm length, 50.08 mm outer diameter and 1.5 mm wall thickness, stainless steel pipe. The pipe has undergone Calcite fouling generation using electrochemistry [4]. Figure 24 shows both pipe specimens before undergoing fouling removal.

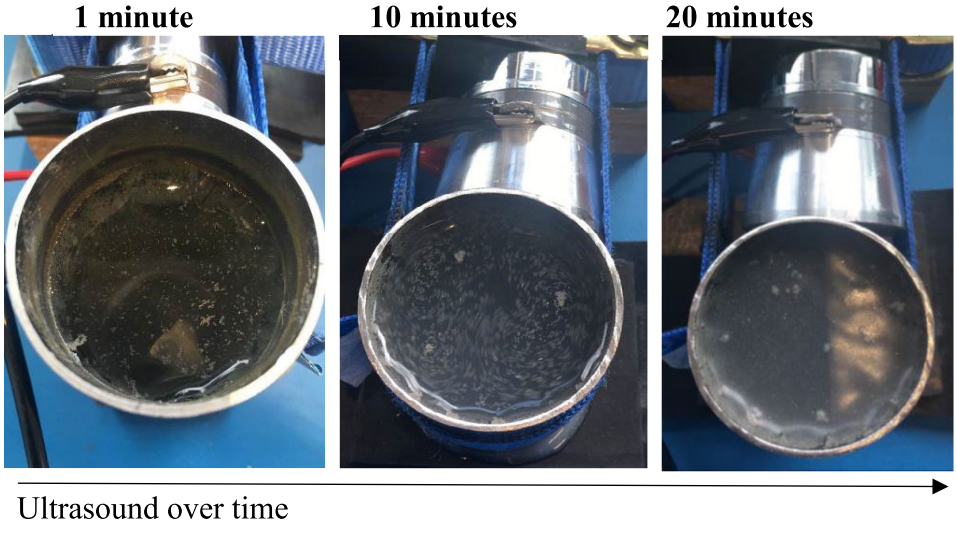

FIGURE 25. HPUT carrying out de-fouling over time.

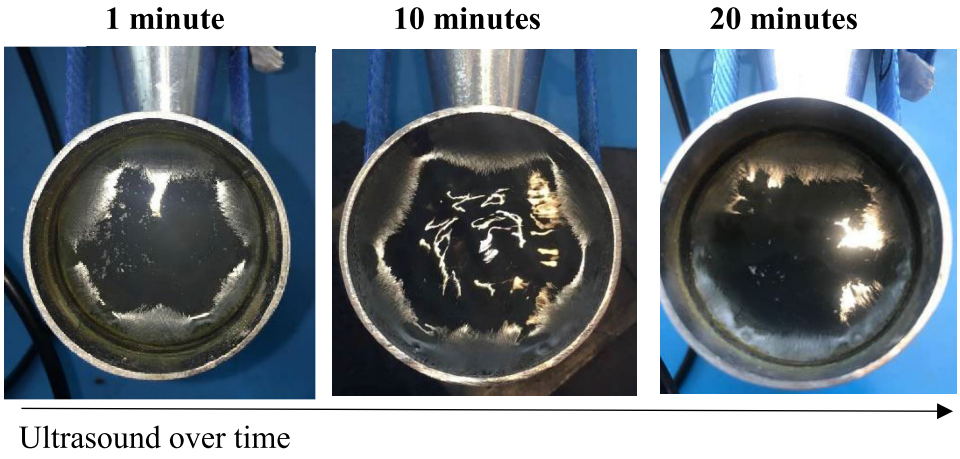

FIGURE 26. Conical sonotrode carrying out de - fouling over time Ultrasound.

Each configuration undergoes fouling removal for 20 minutes for comparison of cleaning coverage over time. Each HPUT is excited using bespoke hardware developed by the Brunel Innovation Centre [35], which inputs a 40 kHz square waveform at 2 amps of current and 200 V.

When exciting the HPUT, cavitation bubbles are generated and over time, the fouling is dislodged into the liquid as shown in Figure 25. For the conical sonotrode, as well as cavitation, high vibration within the liquid can be seen in Figure 26 across the circumference of the inner pipe wall. Figure 27 illustrates the angle of photography to be taken of the pipe specimens for comparison of cleaning coverage.

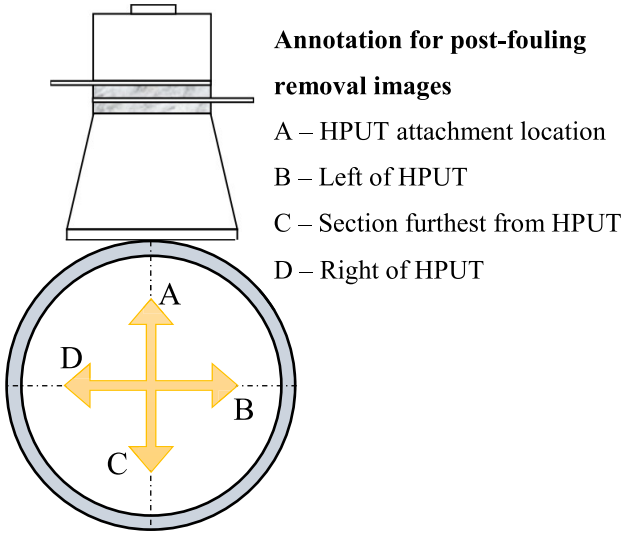

FIGURE 27. Illustration of sectional images for de - fouling analysis Ultrasound.

Figure 28 compares the fouling removal on the inner wall of the pipe specimen at the HPUT attachment location. This is where highest fouling removal is expected, as the HPUT has a larger front mass diameter which allows more contact with the pipe whereas the diameter of the conical sonotrode is

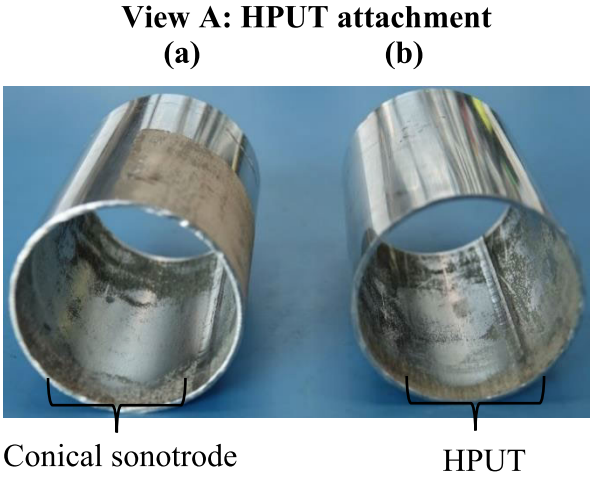

FIGURE 28. View A - HPUT attachment location for (a) conical sonotrode and (b) HPUT.

half the size of the HPUT. The conical sonotrode has shown to achieve a larger surface of cleaning compared to the HPUT, even with a smaller diameter contact surface, due to the half wavelength sonotrode design amplifying the HPUT vibration and delivery into the pipe structure.

From rotating the pipe specimens, Figure 29 displays the propagation of cleaning away from the HPUT location. The conical sonotrode achieves cleaning that is elongated along the length of the pipe, whereas the HPUT has shown cleaning along the length of the pipe but consisting of nodal cleaning with remaining patches of fouling.

The section of the pipe specimens furthest from the HPUT location is shown in Figure 30. Similar to the pipe walls near the HPUT location, there is cleaning along the length of the pipe. The conical sonotrode shows nodes of cleaning but with some locations of fouling remaining in between the nodes, which can be explained by a reduction in vibration across the circumference of the pipe. The HPUT shows the propagation of three nodes of cleaning along the length of the pipe but with

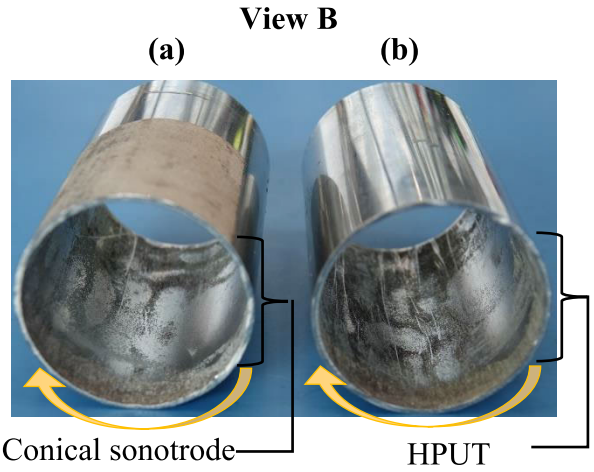

FIGURE 29. View B section for (a) conical sonotrode and (b) HPUT.

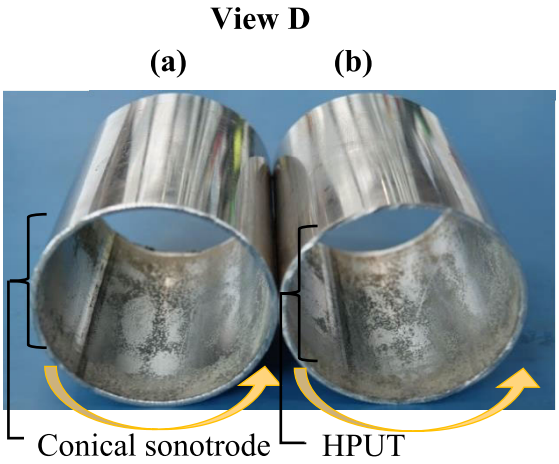

FIGURE 31. View D for (a) conical sonotrode and (b) HPUT.

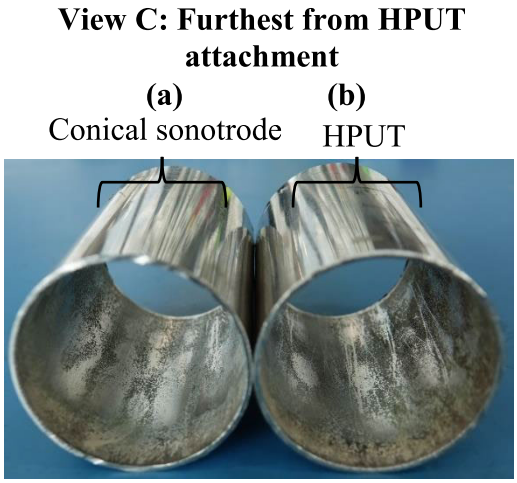

FIGURE 30. View C – section of pipe furthest from HPUT excitation for (a) conical sonotrode and (b) HPUT.

a larger spacing compared to Figure 29, which is also due to a reduction of vibration delivery to this section of the pipe. Figure 31 shows the final section of the pipe near the HPUT location, displaying the propagation of cleaning nodes along the circumference and length of the pipe.

D. COMPARISON OF NUMERICAL AND EXPERIMENTAL FINDINGS

A comparison with the experimental cleaning results for the HPUT attachment shows sets of three nodes propagating before developing into a nodal set of four at the furthest section of the pipe (Figure 22). This shows a good agreement of fouling removal patterns whilst also achieving the minimum pressure required to surpass the cavitation threshold.

Similar to the FEA and cleaning results of the HPUT case, Figure 23 shows that the conical sonotrode also has good agreement of the cleaning patterns with the experimental cleaning results whilst also surpassing the cavitation threshold. When comparing the FEA results for both cases, the conical sonotrodes achieve higher displacement across the pipe and higher total acoustic pressure at the interface of the inner pipe wall, which supports the improved cleaning found from the experimental investigation. When analysing the isosurface of the total acoustic pressure, the HPUT generates pressure fields into the liquid medium whereas the conical sonotrode produces a distribution of pressure field along the inner wall of the pipe. As the experiments had shown the HPUT to generate cavitation, this can be due to the HPUT delivering high pressure into the liquid medium from the attachment location. The conical sonotrode has also produced cavitation during the fouling removal cycle but more distinctively, had generated higher vibrations along the circumference of the inner pipe wall. This could be explained by the delivery of vibration from the horn which does not only focus at the attachment point, and instead, allows the vibration to propagate across the structure which then delivers high pressure into the liquid. This gives an insight into focusing the cavitation generation at the solid-fluid interface without requiring the entire fluid domain to generate cavitation.

VII. CONCLUSIONS AND FURTHER WORK

This work investigated four ultrasonic horn designs (cylindrical, conical, exponential and stepped) tailored for a 40 kHz HPUT to study the potential wave propagation across a 300 mm $\times$ 300 mm $\times$ 2 mm carbon steel plate. The work has shown that, with the attachment of the ultrasonic horn, there is an increase in out of plane displacement at the transducer location. As validated in previous studies by the present authors, this feature is important for designing and optimizing ultrasonic cleaning applications as it can enhance the generation of acoustic cavitation bubbles. A factor that must be accounted for at the transducer location is the displacement in the x and y directions, which will contribute to the wave travelling along the plate structure. From the study, the conical horn has shown the most improvement of the wave propagation (300%) while the stepped horn shows a 30% reduction in wave propagation.

The experimental and numerical cleaning results have shown that the additional conical horn has improved the cleaning achieved during a single cleaning cycle. With this knowledge, further design and optimization can be carried out for improving the HPUT performance for fouling removal purposes as well as for other applications, *i.e.* material processing. For example, the effects due to the *magnitude* of the ultrasonic tip can be investigated by reducing and/or enlarging the tip, combining different horn shapes and selecting ultrasonic horn materials.

VIII. ACKNOWLEDGMENT

The authors would like to thank Adrian Waka, Bradley Woods, and Aristeidis Chatzaroulas of Brunel University London and Mahesh Dissanayake of London South Bank University for their contributions to this article.

REFERENCES

[1] A. S. Paipetis, T. E. Matikas, D. G. Aggelis, and D. Van Hemelrijck, *Emerging technologies in non-destructive testing V*. Boca Raton, FL, USA: CRC Press, 2012.

[2] L. Yang, H. Fu, H. Liang, Y. Wang, G. Han, and K. Ling, "Detection of pipeline blockage using lab experiment and computational fluid dynamic simulation," *J. Petroleum Sci. Eng.*, vol. 183, Dec. 2019, Art. no. 106421.

[3] H. Lais, P. S. Lowe, J. Kanfoud, and T.-H. Gan, "Application of high power ultrasonics for fouling removal in submerged structures," in *Proc. IEEE/MTS OCEANS Conf., Aberdeen*, Aberdeen, U.K., Jun. 2017, pp. 1–8.

[4] H. Lais, P. S. Lowe, T.-H. Gan, and L. C. Wrobel, "Numerical modelling of acoustic pressure fields to optimize the ultrasonic cleaning technique for cylinders," *Ultrason. Sonochem.*, vol. 45, pp. 7–16, Jul. 2018.

[5] H. Lais, P. S. Lowe, J. Kanfoud, and T.-H. Gan, "Advancements in fouling removal using high power ultrasonics for industrial applications," in *Proc. IEEE Int. Conf. Ind. Inf. Syst. (ICIIS)*, Dec. 2017, pp. 1–6.

[6] H. Lais, P. Lowe, T.-H. Gan, L. Wrobel, and J. Kanfoud, "Characterization of the use of low frequency ultrasonic guided waves to detect fouling deposition in pipelines," *Sensors*, vol. 18, no. 7, p. 2122, Jul. 2018.

[7] H. Lais, P. S. Lowe, T.-H. Gan, and L. C. Wrobel, "Numerical investigation of design parameters for optimization of the *in-situ* ultrasonic fouling removal technique for pipelines," *Ultrason. Sonochem.*, vol. 56, pp. 94–104, Sep. 2019.

[8] *Hilsonic*. Accessed: Aug. 14, 2017. [Online]. Available: http://www.hilsonic.co.uk/

[9] *Ultrawave*. Accessed: Aug. 14, 2017. [Online]. Available: http://www.ultrawave.co.uk/

[10] H. Maddah and A. Chogle, "Biofouling in reverse osmosis: Phenomena, monitoring, controlling and remediation," *Appl. Water Sci.*, vol. 7, no. 6, pp. 2637–2651, Oct. 2017.

[11] H.-C. Flemming, "Reverse osmosis membrane biofouling," *Exp. Therm. Fluid Sci.*, vol. 14, no. 4, pp. 382–391, May 1997.

[12] G. Harvey, A. Gachagan, and T. Mutasa, "Review of high-power ultrasound-industrial applications and measurement methods," *IEEE Trans. Ultrason., Ferroelectr., Freq. Control*, vol. 61, no. 3, pp. 481–495, Mar. 2014.

[13] T. J. Mason, "Ultrasonic cleaning: An historical perspective," *Ultrason. Sonochem.*, vol. 29, pp. 519–523, Mar. 2016.

[14] N. I. Marinescu, D. Ghiculescu, and O. Alupei, "Aspects concerning FEM modelling of an ultrasonic horn used at micro-EDM drilling," *Nonconventional Technol. Rev.*, vol. 20, no. 4, pp. 31–36, Dec. 2016.

[15] A. S. Nanu, N. I. Marinescu, and D. Ghiculescu, "Study on ultrasonic stepped horn geometry design and FEM simulation," *Nonconventional Technol. Rev.*, vol. 4, pp. 25–30, Dec. 2011.

[16] K.-M. Shu and J.-W. Chen, "The design of acoustic horns for ultrasonic aided tube double side flange making," *Int. J. Mech., Aerosp., Ind., Mechatronic Manuf. Eng.*, vol. 9, no. 5, pp. 1–4, Jun. 2015.

[17] Y.-J. Choi, K.-H. Park, Y.-H. Hong, K.-T. Kim, S.-W. Lee, and H.-Z. Choi, "Effect of ultrasonic vibration in grinding; horn design and experiment," *Int. J. Precis. Eng. Manuf.*, vol. 14, no. 11, pp. 1873–1879, Nov. 2013.

[18] M. R. Rani and R. Rudramoorthy, "Computational modeling and experimental studies of the dynamic performance of ultrasonic horn profiles used in plastic welding," *Ultrasonics*, vol. 53, no. 3, pp. 763–772, Mar. 2013.

[19] M. Nad', "Ultrasonic horn design for ultrasonic machining technologies," *Appl. Comput. Mech.*, vol. 4, no. 1, pp. 68–78, 2010.

[20] S. Lin, "Analysis of multifrequency Langevin composite ultrasonic transducers," *IEEE Trans. Ultrason., Ferroelectr., Freq. Control*, vol. 56, no. 9, pp. 1990–1998, Sep. 2009.

[21] D. M. Donskoy and B. A. Cray, "Acoustic particle velocity horns," *J. Acoust. Soc. Amer.*, vol. 131, no. 5, pp. 3883–3890, Mar. 2012.

[22] P. Harkness, M. Lucas, and A. Cardoni, "Coupling and degenerating modes in longitudinal–torsional step horns," *Ultrasonics*, vol. 52, no. 8, pp. 980–988, Dec. 2012.

[23] A. Mathieson, N. Cerisola, and A. Cardoni, "Nonlinear characterization of half and full wavelength power ultrasonic devices," *Phys. Procedia*, vol. 87, pp. 125–131, Jan. 2016.

[24] V. Raman, A. Abbas, and S. C. Joshi, "Mapping local cavitation events in high intensity ultrasound fields," in *Proc. Excerpt COMSOL Users Conf.*, Bangalore, India, 2006, pp. 1–6.

[25] V. S. Sutkar, P. R. Gogate, and L. Csoka, "Theoretical prediction of cavitational activity distribution in sonochemical reactors," *Chem. Eng. J.*, vol. 158, no. 2, pp. 290–295, Apr. 2010.

[26] S. L. Peshkovsky and A. S. Peshkovsky, "Matching a transducer to water at cavitation: Acoustic horn design principles," *Ultrason. Sonochem.*, vol. 14, no. 3, pp. 314–322, Mar. 2007.

[27] Z. Wei, J. A. Kosterman, R. Xiao, G.-Y. Pee, M. Cai, and L. K. Weavers, "Designing and characterizing a multi-stepped ultrasonic horn for enhanced sonochemical performance," *Ultrason. Sonochem.*, vol. 27, pp. 325–333, Nov. 2015.

[28] L. E. Kinsler, A. R. Frey, A. B. Coppens, and J. V. Sanders, "Fundamentals of acoustics," in *Fundamentals of Acoustics*, Lawrence E. Kinsler, Austin R. Frey, Alan B. Coppens, James V. Sanders, 4th ed. Hoboken, NJ, USA: Wiley-VCH, Dec. 1999, p. 560.

[29] S. H. Kristensen, "Design, construction and characterization of high power ultrasound sources," M.S. thesis, Univ. Southern Denmark, Sønderborg, Denmark, 2009.

[30] *Augment Your COMSOL Multiphysics Models With Material Properties From the Material Library*. Accessed: May 18. 2019. [Online]. Available: https://uk.comsol.com/material-library

[31] *Resolving Time-Dependent Waves*. Accessed: Jun. 11, 2016. [Online]. Available: https://www.comsol.com/support/knowledgebase/1118/

[32] *4294A Precision Impedance Analyzer*. Accessed: May 18, 2019. [Online]. Available: https://www.keysight.com/gb/en/home.html

[33] *Beijing Ultrasonics*. Accessed: Aug. 7, 2019. [Online]. Available: https://www.bjultrasonic.com/

[34] *Polytec PSV-400 3D Laser Scanning Vibrometer*. Accessed: May 18, 2019. [Online]. Available: https://www.polytec.com/uk/

[35] *Brunel Innovation Centre*. Accessed: Aug. 4, 2019. [Online]. Available: https://www.brunel.ac.uk/bic

HABIBA LAIS received the B.Eng. degree (Hons.) in aerospace engineering with professional development from Brunel University London, in 2016. She was a Project Technical Assistant with the Brunel Innovation Centre (BIC), from 2014 to 2015. She has joined BIC as a Research Assistant to continue her research in ultrasonic cleaning for off-shore applications. Upon graduating, she returned to BIC as an NSIRC Ph.D. Student (funded by EPSRC and accredited by Brunel University London) to continue research in non-invasive fouling removal using ultrasonics whilst assisting on related Innovate UK projects. During the time at BIC, she involved in fouling removal projects using high power ultrasonic transducers. She has authored several peer-reviewed journals and conference papers. Her current research interests include ultrasonic transducers, vibration analysis, simulations and bubble dynamics.

PREMESH SHEHAN LOWE (S'13–M'16) received the Ph.D. degree in electrical and computer engineering, specializing in ultrasonic sensor development for non-destructive testing from Brunel University London, Uxbridge, U.K., in 2016. From 2012 to 2015, he was a Ph.D. Research Engineer with TWI Ltd., Cambridge, U.K. From 2015 to 2019, he was the Team Lead/Research Fellow in power ultrasonic with the Brunel Innovation Centre, Cambridge, U.K. His research at the Brunel Innovation Centre was focused on the development of sensors for in-situ structural health monitoring and power ultrasonic applications. He is currently a Nuclear NDE Research Engineer with Nuclear AMRC, Sheffield, U.K. He has authored or coauthored more than 25 peer-reviewed journals and conferences. His current research interests include the development of sensors and sensor networks to assess the structural integrity of aging nuclear power plants. He is an executive member of the IEEE UK&I Section and serving as the Chapter Officer, since 2017. He received the Exemplary Award for his service in the IEEE UK&I Section, in 2018. He has been serving the scientific community as a Reviewer for the IEEE Journals, NDT&E, and *Sensors* Journal, since 2014.

LUIZ CARLOS WROBEL is currently a part-time Professor with the Department of Mechanical and Aerospace Engineering, Brunel University London, U.K., and also a Professor with the Department of Civil and Environmental Engineering, Pontifical Catholic University of Rio de Janeiro (PUC-Rio), Rio de Janeiro, Brazil. He is a member of the Board of the Brunel Innovation Centre, TWI, Cambridge, U.K., and a member of the Oil and Gas Board, Institute of Materials, Minerals and Mining, U.K. He supervised 18 postdoctoral research fellows, 37 Ph.D., five M.Phil., and 33 M.Sc. theses successfully defended, and currently supervise five Ph.D. students. He is the author or coauthor of four books on *Numerical Methods* in engineering, one of which was translated to Japanese, Russian, and Chinese. He contributed 26 chapters to edited books, and published 184 articles in international journals and 266 conference papers. His current research interest includes structural integrity and energy.

TAT-HEAN GAN received the degree (Hons.) in electrical and electronics engineering from the University of Nottingham, the M.Sc. degree (Hons.) in advanced mechanical engineering from the University of Warwick, in 1998, where he is currently pursuing the Ph.D. degree in engineering specializing in advanced ultrasonic imaging, and the Executive MBA degree from the University of Birmingham.

He has academic and industry experience for many years. He is currently a Professor with Brunel University London, where he is also the Professor of structural integrity with the College of Engineering, Design and Physical Sciences. He is currently the Director of innovation and skills with TWI Ltd., and the Brunel Innovation Centre (BIC). He is also the Technology Director of the National Structural Integrity Research Centre (NSIRC), the UK's first industry-led postgraduate education and research center in structural integrity, which is based at TWI. He is a Visiting Professor with the Dalton Nuclear Institute, University of Manchester, U.K., Tianjin University, China, and the Wuhan University of Technology, China. Recently, he has been appointed as the Chair of the Non-metallic Innovation Centre (NIC), collaboration between TWI, Saudi Aramco Technologies, and ADNOC, to develop flexible pipe composites for oil and gas applications. He has published more than 100 articles and has contributed to several books in the field of non-destructive testing (NDT). His current research interests include signal and image processing, sensor development, artificial intelligence, digital twin, asset integrity management, and structural assessment.

Dr. Gan is a Fellow of the Institute of Engineering and Technology, the British Institute of Non-Destructive Testing, the International Society of Condition Monitoring, the International Society of Engineering Asset Management, and the Welding Institute. He was a recipient of the Welding Institute Lidstone Award, who is deemed to have made the most significant contribution to the advancement of welding technology. He received the CEng, EurIng, and IntPE(UK) status.